IEEE Access
Multidisciplinary | Rapid Review | Open Access Journal

Received July 7, 2020, accepted August 2, 2020. Date of publication xxxx 00, 0000, date of current version xxxx 00, 0000.

Digital Object Identifier 10.1109/ACCESS.2020.3014498

Performance Improvement of Existing Three Phase Synchronous Reluctance Machine: Stator Upgrading to 5-Phase With Combined Star-Pentagon Winding

KOTB B. TAWFIQ [1,2,3], MOHAMED N. IBRAHIM [1,2,4], (Member, IEEE), E. E. EL-KHOLY [3], (Member, IEEE), AND PETER SERGEANT [1,2], (Senior Member, IEEE)

[1]Department of Electromechanical, Systems, and Metal Engineering, Ghent University, 9000 Ghent, Belgium
[2]Core Lab EEDT-MP, FlandersMake@UGent, 3001 Leuven, Belgium
[3]Department of Electrical Engineering, Faculty of Engineering, Menoufia University, Menoufia 32511, Egypt
[4]Department of Electrical Engineering, Kafrelshiekh University, Kafrelshiekh 33511, Egypt

Corresponding author: Kotb B. Tawfiq (kotb.basem@ugent.be)

This work was supported by the Special Research Fund of Ghent University (BOF), Belgium.

ABSTRACT This paper investigates the performance of 3-phase synchronous reluctance machines (SynRMs) when upgrading their stator to 5-phase, keeping the same rotor. The design of the 5-phase stator has been optimized to select the optimal dimensions of the slots and teeth. Moreover, a combined star-pentagon winding is employed to further improve the machine performance. Different winding configurations have been studied and compared using 2D Ansys Maxwell transient simulations. It is observed that at optimal current angle and rated current, the average torque is increased by 17.41% when changing the 3-phase stator with the proposed 5-phase one. In addition, the efficiency of the 5-phase SynRM is increased by about 0.8% compared to 3-phase SynRM. At 3 times the rated speed, the torque and efficiency are significantly increased by around 33% and 3.5% respectively. Moreover, the 5-phase SynRM shows a superior performance in the faulty case with one phase opened. It works at 98.84% of the rated torque of the healthy 3-phase machine, whereas the 3-phase machine works at only 43.35% with huge torque ripple (228%). Finally, an experimental validation using the reference 3-phase machine has been done.

INDEX TERMS Combined star-pentagon, FEM, multiphase machines, optimization, synchronous reluctance motor.

NOMENCLATURE

a_c	Conductor cross-sectional area
A_{s3}	Stator slot area for 3-phase machine
A_{s5}	Stator slot area for 5-phase machine
b_{s0}	Slot width at opening
b_{s1}	Slot width at top conductor
b_{s2}	Slot width at bottom
b_{t0}	Teeth width at tip
b_{tb}	Teeth width at bottom
D	Stator inner diameter
D_{o1}	Stator outer diameter
h_{s0}	Slot opening height
h_{s1}	Slot height above conductors
h_{s2}	Slot copper height
h_{s3}	Slot bottom height
$i_{A,B,C,D,E}$	Stator phase currents
$i_{d,q}$	Direct and quadrature axis current
K_f	Slot filling factor
K_s	Park and Clark transformation matrix
$L_{d,q}$	Direct and quadrature axis inductance
N_{c3}	Number of conductors per slot for 3-phase
N_{c5}	Number of conductors per slot for 5-phase
P	Number of pole pairs
PF	Power factor
R_s	Stator phase resistance
S	Stator slots number
T_m	Electromagnetic torque

The associate editor coordinating the review of this manuscript and approving it for publication was Bijoy Chand Chatterjee.

T_r	Torque ripple percentage value
$V_{d.q}$	Direct and quadrature axis voltage
$\lambda_{d.q}$	Direct and quadrature axis flux linkage
ω	Angular rotor position
θ_r	Rotor position
α	Current angle
Φ	Power factor angle

I. INTRODUCTION

The clear trend in power industrial fields is to have an electric machine with a higher efficiency and improved torque density. This can be obtained by reducing the losses in electric machine and/or enhancing the winding factor and the magneto motive force (MMF). The losses in synchronous reluctance machines (SynRMs) are lower compared to induction machines and permeant magnet synchronous machines [1], [2]. This is due to the absence of windings, permanent magnets and cage in their rotors. Therefore, they have lower rotor temperature rise compared to other electrical machines [3]. Hence, the efficiency and the cost of SynRMs are promising compared to other electric machines. Therefore, SynRMs have been receiving a great interest to be employed in high power industrial fields [4].

The performance of SynRMs largely depends on their saliency ratio (the ratio between direct and quadrature axis inductance) [5]. This ratio depends on rotor geometrical parameters, stator geometry, magnetic materials and winding type [6]. Hence, Modification in any of these parameters will have an impact on the SynRM's performance. Many researches have been conducted to improve SynRM's performance (increase average torque and efficiency and reduce torque ripple) using different stator winding type [3], magnetic material [5] and flux barrier geometry [7]–[10]. It has been found in [7]–[10] that the rotor geometry is largely affected by number of stator slots.

Thanks to their higher fault tolerance property and reliability, multiphase machines (>3-phases) have been recently gaining popularity in some industrial applications in which reliability is a key element e.g. in military, aerospace and hospital [11], [12]. Further, multiphase machines have higher torque density and lower current rating compared to three phase machines [13]. Hence, an improved performance of SynRMs can be achieved using higher number of phase due to the enhancement in winding factor and the MMF. In order not to increase the size of power converter and complicate the control system, most of scientific researches focus on 5-phase winding over other multiphase windings [14].

There are two possibilities to obtain a 5-phase SynRM from an existing 3-phase SynRM. The first possibility is to apply the 5-phase winding to the existing 3-phase stator. This way is the lowest cost strategy as only the winding will be changed. However, unfortunately, a simple and balanced 5- phase winding might not be possible from the existing 3-phase stator. This is because, most of the existing 3-phase stators were manufactured to give an integer number of slots per pole per phase with 3-phase winding (18, 24, 36 or 48-slots and 2, 4 or 6-poles) [15]. Consequently, a fractional number of slots per pole per phase will be obtained when applying a 5-phase winding to these stators. Hence, a complex special winding with increased cost is required to obtain a balanced 5-phase winding from the existing 3-phase stator. The second possibility is to keep the existing rotor and replace the existing 3-phase stator by another one that can give an integer number of slots per pole per phase (20, 40 or 60 slots). Hence, the simple conventional winding methods can be applied. However, there is some difficulty in this option as the rotor geometry was previously optimized based on the existing 3-phase stator and the SynRM performance will be affected. Hence, the first contribution in this paper is to optimize the design of the 5-phase stator, keeping the existing three phase machine rotor to realize an improved 5-phase SynRM.

The 5-phase winding can be connected either in star, pentagon or pentacle as depicted in fig.1 [16]. Star connected windings have shown better performance especially during the healthy case and the pentagon and pentacle configurations are better during the faulty case [16]–[19]. The winding changeover between star, pentagon and pentacle configurations for a 10 A, 15 slot and 4 poles 5-phase permanent magnet synchronous machine was studied in [16] and it was proved that the motor could have a wide operational speed range. The changeover between star and pentagon windings represents a big drawback for any drive system. The combined connection between star and pentagon is recently used as it combines both advantage of star and pentagon configurations [17]–[19]. In [17] a combined star-pentagon winding for a 1.1 kw, 40 slot and 4 poles 5-phase induction motor was introduced. The proposed winding provides higher efficiency with better flux distributions at healthy case and lower derating factor for faulty case. The dynamic and steady state modelling for the combined star-pentagon winding for a 1.1 kw, 40 slot and 4 poles 5-phase induction motor were presented in [18], [19].

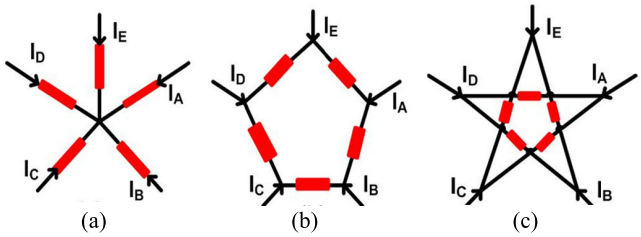

FIGURE 1. Five phase winding configurations, (a) Star, (b) Pentagon and (c) Pentacle.

To the best of author's knowledge, in the literature, the implementation of a combined star-pentagon configuration to a 5-phase SynRM is not investigated. Therefore, the combined start-pentagon configuration will be applied to the optimized 5-phase SynRM. It is expected that the proposed 5-phase SynRM wound by the combined star- pentagon will result in an improved torque density and efficiency compared to the existing SynRMs in the literature.

II. STATOR DESIGN AND OPTIMIZATION

Most of the recent research in multiphase machines focuses on the odd phase number, e.g. five and seven phases, because the higher MMF harmonics of the even phase numbers results in increased torque ripple and losses [20], [21]. Hence, this section investigates the performance of SynRM by replacing the 3-phase stator iron and winding to a 5-phase winding, keeping the same rotor to minimize the cost. The 5-phase is chosen so as not to increase the size of the power converter and complicate the control system. Some analysis for MMF magnitude and harmonics as well as the winding factor is carried out in this section. Besides, an optimization technique is applied to select the optimized geometry design of the upgraded stator with the existing rotor which gives a 5-phase SynRM with improved performance (high efficiency and average torque and low torque ripple).

A. NUMBER OF STATOR SLOTS SELECTION

The optimal number of stator slots and winding details for the 5-phase stator will be selected based on the analysis of the MMF and winding factor of various numbers of stator slots. Current density, copper and iron volume are kept fixed as much as possible as in the 3-phase stator. The number of conductors per slot of the 5-phase SynRM is calculated based on the 3-phase machine, keeping the same copper volume as much as possible, as follows:

$$N_{c5} * S_5 = N_{c3} * S_3 \tag{1}$$

There are two major constraints for the upgraded 5-phase stator to be used with the existing rotor: 1) similar stacking length and 2) similar stator bore diameter. The second constraint limits the available number of slots that can be used. The stator of the existing 3-phase SynRM (reference machine) has S_3 slots. The possible numbers of slots for the 5-phase stator considering saturation and mechanical problems will be calculated from (2). The integral slot distribution winding is only considered in this formula. Table 1 displays the range of the number of slots of the 5-phase stator for different number of rotor poles and different numbers of stator slots of the 3-phase machine.

$$S_5 = \frac{q_5 * 5 * S_3}{3 * q_3}$$
$$q_5 = 1, 2, 3, \ldots\ldots, q_3 \quad \text{and } S_5 \leq 2S_3 \tag{2}$$

A case study of a 5.5 kW SynRM with 4 poles, 36-slots and 26 conductors per slot 3-phase SynRM (introduced in [22], [23]), is studied. The rotor of the reference SynRM was optimized with its stator in [22] to obtain an improved performance. A rotor with 4-poles is selected as it has been proved in [24] that a 4-poles rotor shows a better performance. Consequently, 20, 40 and 60 slots are the possible number of slots of the 5-phase stator which achieve the constrains of (2) and Table 1. A 20-slots 5-phase stator will not be considered in the next parts of this paper as it has the highest MMF harmonics as shown in Table 2. It is seen from Table 2 and fig. 2(a, b) that 40-slots (5-phase) has lower MMF harmonics

TABLE 1. The permissible numbers of slots for the new five phase stator for different number of slot per pole per phase.

S_3	q_3	Range of S_5
12	2	10, 20
	1	20
18	3	10, 20, 30
	1	30
24	4	10, 20, 30, 40
	2	20, 40
	1	40
36	6	10, 20, 30, 40, 50, 60
	3	20, 40, 60
	2	30, 60
48	8	10, 20, 30, 40, ..., 80
	4	20, 40, 60, 80
	2	40, 80
60	10	10, 20, 30, 40, ...,100
	5	20, 40, 60, 80, 100

TABLE 2. Analysis of MMF and winding factor.

n	S	Winding Factor	Fundamental MMF (PU)	% THD in MMF	% Increase in copper
3	36	0.9598	1	9.88	base
5	20	1	1.0686	16.38	2.56
	40	0.9877	1.0555	7.473	2.56
	60	0.9854	1.053	3.972	1.71

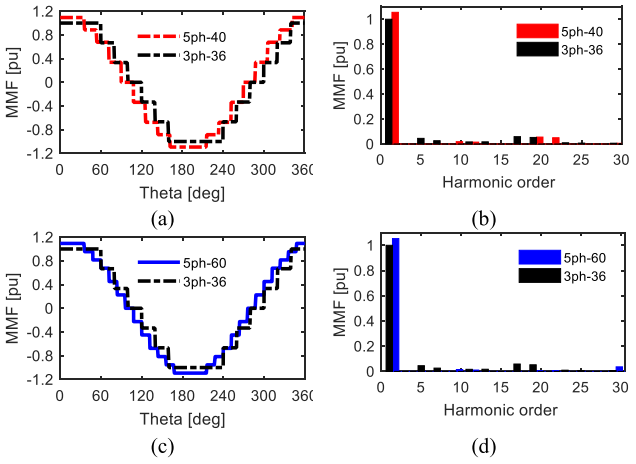

FIGURE 2. Analysis of MMF of 5-phase SynRM with 40 and 60-slots.

compared to the 3-phase machine and also a higher winding factor. Figure 2(c, d) shows that 60-slots (5-phase) has the lowest MMF harmonics. Therefore, an improved 5-phase SynRM could be achieved with 40 and/or 60-slots.

B. OPTIMIZATION OF STATOR DIMENSIONS

In this section, the stator of the two 5-phase SynRMs (40 and 60-slots) have been optimized and the performance of the two SynRMs is compared with the 3-phase machine, keeping the same rotor. Similar axial length, stator diameters, air gap length and slot filling factor of the 3-phase machine stator

has been employed in case of 5-phase stators. Consequently, only the dimensions of the teeth and the slot (slot opening, slot width at top and bottom and slot depth) should be designed to achieve an optimized performance 5-phase SynRM. Figure 3(a) shows the stator teeth and slot dimensions. The slot opening width can be calculated using teeth width at tip from (3). Using the slot width at the bottom, the teeth width at the bottom can be calculated from (4). The third geometrical parameter of the slot is calculated from (5). The slot depth is controlled from (6) so that the slot area of the 5-phase SynRM should have the same filling factor of the 3-phase machine as in (7) and (8). This is due to the using of the same copper volume for both three and five-phase SynRMs. The slot filling factor (K_f) of the existing three-phase SynRM is 0.405.

$$b_{s0} = \frac{\pi * D}{S} - b_{t0} \tag{3}$$

$$b_{tb} = \frac{\pi * (D + 2h_{s0} + 2h_{s1} + 2h_{s2})}{S} - b_{s2} \tag{4}$$

$$b_{s1} = \frac{\pi * (D + 2h_{s0} + 2h_{s1})}{S} - b_{tb} \tag{5}$$

$$h_{s2} = \frac{2A_{s5} - (b_{s0} + b_{s1}) * h_{s1} - 2b_{s0}h_{s0} - 2b_{s2}h_{s3}}{(b_{s1} + b_{s2})} \tag{6}$$

$$N_{c5} * a_c = K_f * A_{s5} \tag{7}$$

$$N_{c3} * a_c = K_f * A_{s3} \tag{8}$$

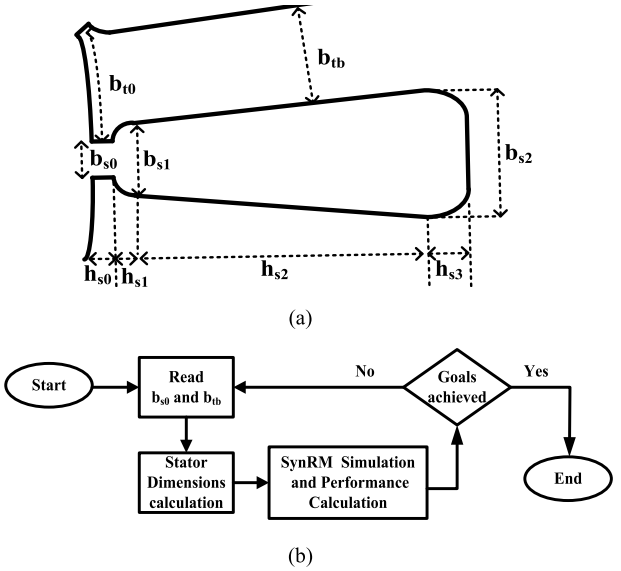

FIGURE 3. (a) Stator slot and teeth dimensions and (b) Flow chart of the optimization technique.

In order to obtain the optimal stator slot and teeth dimensions for the considered multiphase stators (40 and 60 slots), an optimization algorithm is used. Optimal design for electric machines based on finite element magnetic simulation consumes a lot of time, therefore, choosing a suitable optimization technique is necessary to obtain an optimal design for the electric machines with a reduced time computation [25]. Multi-objective optimization or Pareto optimization has proved its efficient in different electrical machine design [26]–[28]. Nelder–Mead method presented in [28] is a multi-objective optimization based on a single criterion method. In this approach, the optimization objectives are grouped to construct this criterion. This will reduce the optimization process time and the calculation effort [28]. Further, this approach can be executed in Matlab using function (*fminsearch*). Consequently, this optimization approach will be applied in this paper to select the optimal dimensions of the 5-phase SynRMs. The optimization goals, variables and constraints are defined in Table 3. The maximum and minimum values of the optimization variables, shown in Table 3, is selected based on the FEM model so as no to complicate the winding process and prevent machine saturation. The flow chart of the optimization process is shown in fig.3(b). The optimization process has three objectives which are grouped to construct a single criterion as in (9). The torque ripple lower than 10 is the first goal and its weighting factor is set to 1 (which is the highest important); the average torque higher than 18.5 N.m is the second goal with weighting factor equal to 0.9; the last goal in the optimization process is efficiency higher than 94.8% and its weighting factor is set to 0.85. Finally, the optimization technique is minimizing the cost function in (9) considering the weighting factors of each objective.

$$cost\ function = 1 * T_r - 0.9 * T_{av} - 0.85 * \eta \tag{9}$$

TABLE 3. Variables, constraints and goals of the optimization technique.

Constraints	Axial length, L	140 mm
	Bore diameter, D	110 mm
	Outer diameter, D_0	180 mm
	Airgap length	0.3 mm
	Slot filling factor	0.405
Variables	Teeth width at bottom, b_{tb}	3.5mm< b_{tb} <6mm (40-slots)
		3mm< b_{tb} <4.5mm (60-slots)
	Slot width at opening, b_{s0}	0.5mm< b_{s0} <3.6mm (40-slots)
		0.5mm< b_{s0} <3.25mm (60-slots)
Goals	Torque ripple, T_r %	< 10%
	Average torque, T_{av}	> 18.5 N.m
	Efficiency, η %	> 94.8%
Weight factor	Torque ripple, T_r	1
	Average torque, T_{av}	0.9
	Efficiency, η	0.85

The result of the optimization of the 5-phase SynRMs (40 and 60-slots) is shown in fig.4 and fig.5 respectively. It has been noted that the average torque is directly proportional with the stator teeth width and inversely proportional with the slot opening. The teeth and slot dimensions have a significant effect on the torque ripple as shown in fig.4 (b) and fig.5 (b). It varies from 9.45% to 36.82% and 4.35% to 13.62% for the 40 and 60-slots stators respectively. Figure 4 (c) and fig.5 (c) show that the total losses increase

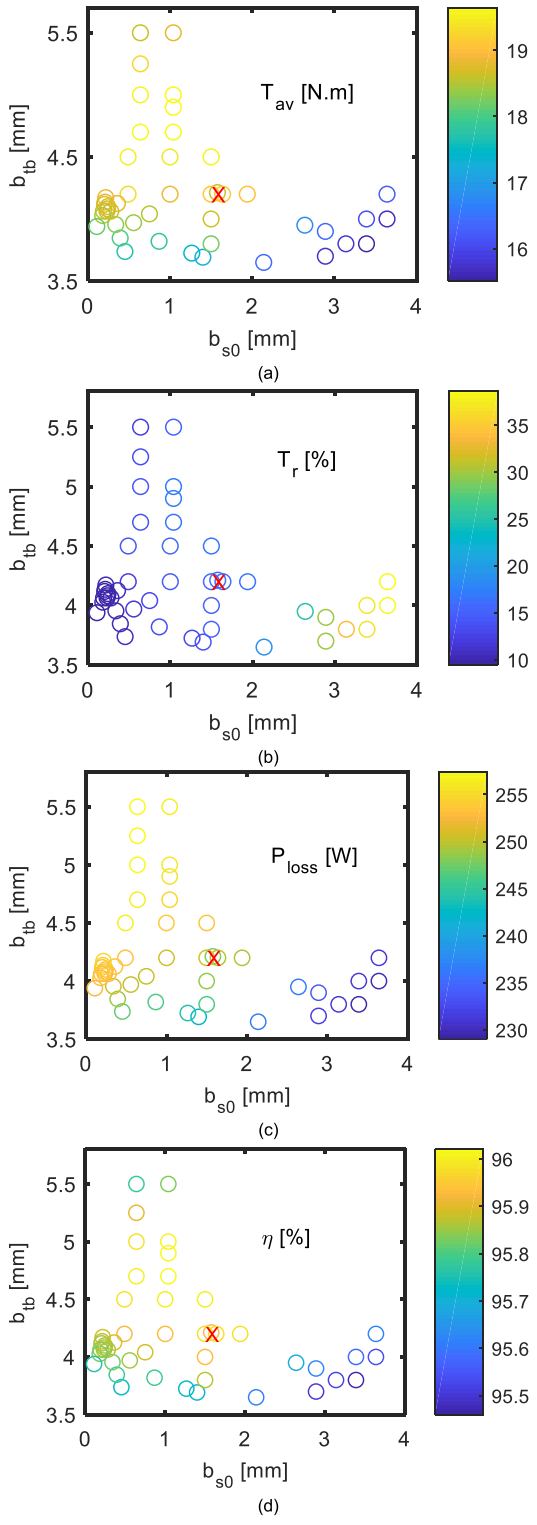

FIGURE 4. Result of the optimization technique result for stator of 40-slots, (a) Average torque, (b) Torque ripple, (c) Total losses and (d) Efficiency.

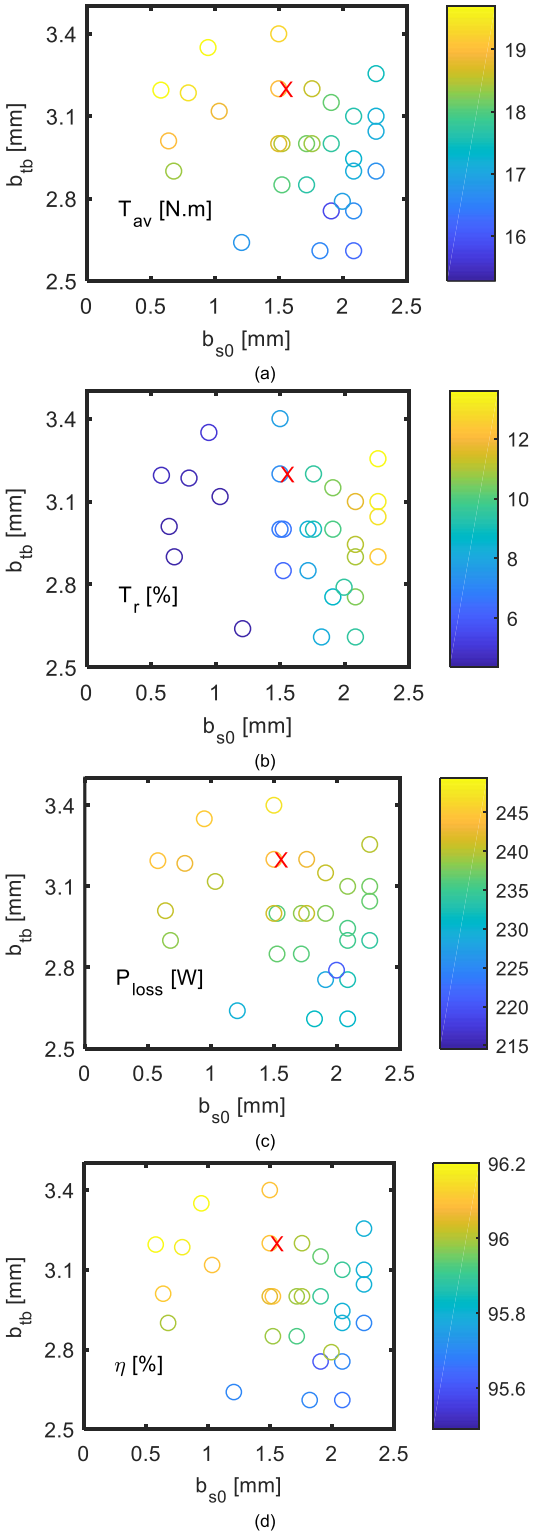

FIGURE 5. Result of the optimization technique result for stator of 60-slots, (a) Average torque, (b) Torque ripple, (c) Total losses and (d) Efficiency.

when the slot opening decreases. This is due to the increase in the iron losses in stator core. The efficiency of the upgraded stators is shown fig.4 (d) and fig.5 (d).

The optimal design of the upgraded stators is selected based on the optimization goals shown in Table 3. The optimal design is signified by the red cross (X) in fig.4 and fig.5.

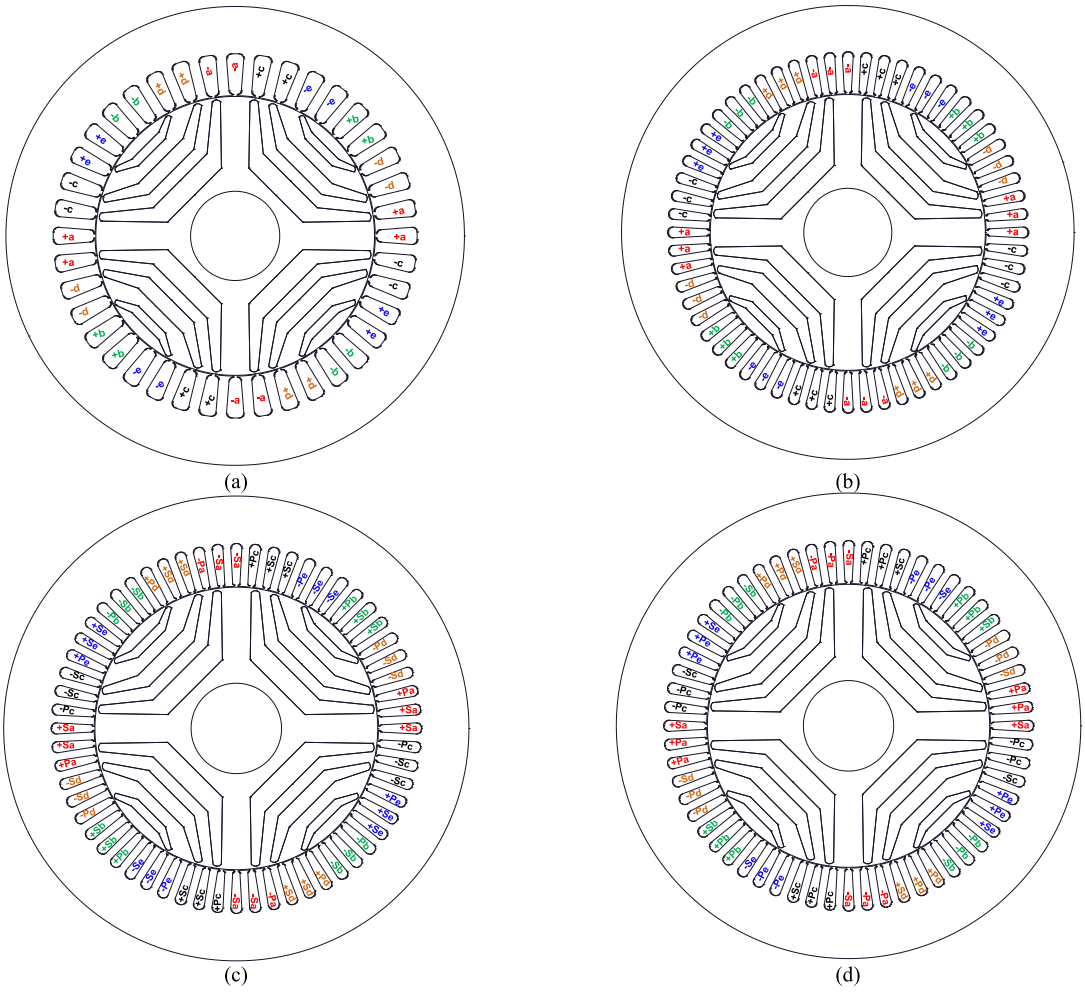

FIGURE 6. Cross-sections of the optimal designs of five-phase SynRMs with different winding configurations (a) 40-slots and star winding, (b) 60-slots and star winding, (c) 60-slots and SSP winding and (d) 60-slots and SPP winding.

The optimal dimensions are (b_{s0} = 1.5 mm, b_{tb} = 4.2 mm and h_{s2} = 12.3 mm) and (b_{s0} = 1.5 mm, b_{tb} = 3.2 mm and h_{s2} = 13.6mm) for the 5-phase 40 and 60-slots stators respectively. Figure 6 shows the cross-sections of the optimal designs with winding configuration on it. Figure 6(a) shows 5-phase SynRM with 40-slots and star connected winding whereas, the 60-slots SynRM with star connected winding is shown in fig.6(b). At the optimal dimensions, it has been found that the average torque and efficiency of the 5-phase SynRMs are improved by 10.3% and 1.16% respectively compared to the 3-phase SynRM. The torque ripple of the 60-slots 5-phase SynRM is reduced by 8.7% compared to the 3-phase SynRM. However, the torque ripple of 40-slots 5-phase SynRM is increased to about double the value of the 3-phase SynRM. From the previous analysis, the optimized 60-slots 5-phase stator gives an improved performance with the existing rotor. Hence, it will be considered in the next sections in this paper.

III. COMBINED STAR-PENTAGON CONFIGURATION

In this section, the effect of winding configurations on the torque producing MMF component of a 60-slot, 4-pole, 5-phase SynRM is studied. The considered 5-phase SynRM has 3 slots per pole per phase. The coils of each phase can be connected in series and the phases could be connected with each other either in star (S) or pentagon (P) connections. A combined star-pentagon connection, which is shown in fig.7, could be used to obtain an improved 5-phase SynRM performance. There are several winding layouts possibilities for the combined star-pentagon with single layer winding as depicted in Table 4 and fig. 6(c, d). The abbreviations SPP, PPS and PSP mean that for three adjacent slots, two slots are assigned to the pentagon-connected winding set and one slot is assigned to the star-connected winding set. The relation between the current of the pentagon winding and the current of the star winding is given by (10). Hence, the cross-sectional area of conductors of the pentagon windings will be smaller than of cross-sectional area of the conductors of star wind-

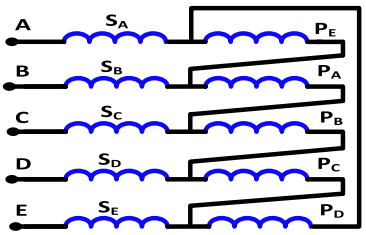

FIGURE 7. Combined star-pentagon connection.

TABLE 4. Winding factor and MMF for different winding configuration of the five phase machines.

n	Connection	MMF Mag. [pu]	% MMF Harmonic	Winding factor
3	Existing	1	9.88	0.9598
5	S	1.0530	3.972	0.9854
	SSP	1.0647	3.581	0.9963
	SPS	1.0414	4.311	0.9854
	SPP	1.0647	3.581	0.9963
	PSS	1.0184	5.0123	0.9963
	PSP	1.0414	4.311	0.9854
	PPS	1.0184	5.013	0.9963

ings. The conductor's cross-sectional area of star connected winding for both three and five-phase SynRM is 1.57 mm^2. Whereas, the cross-section area for the pentagon winding is 1.31 mm^2.

$$x_{star} = 2\sin\frac{\pi}{5}x_{pentagon} = 1.1756x_{pentagon}$$
$$x \text{ represents current or cross-sectional area} \qquad (10)$$

Consequently, the number of turns of the pentagon winding ($N_{pentagon}$) has to be higher than the number of turns of the star winding (N_{star}) to obtain the same MMF from both windings [17]. The relation between the numbers of turns can be given by (11). Hence, there will be no change in losses when converting some winding from star to pentagon connection.

$$N_{pentagon} = 1.1756N_{star} \qquad (11)$$

The number of conductors per slot of the star winding of the 5-phase SynRM has been previously selected based on (1) and its value is 16. Hence, the number of conductors per slot of the pentagon winding will be 19 and the filling factor of the slot will be the same. Table 4 and fig.8 show that the SSP and SPP layouts have the highest MMF magnitude and the lowest MMF harmonics using the same copper volume. The MMF magnitude is increased with these layouts by 6.47% and the harmonic content of the MMF is reduced by about 64% compared to the 3-phase SynRM. The increase of the winding factor and the magnitude of the MMF of the 5-phase SynRM helps to obtain an improved torque density compared to the existing 3-phase machine with the same cost. Consequently, the efficiency of the machine could be increased as well.

Figure 9 shows the star of slot phasors of both the terminal voltage and the induced voltage across each coil for different winding layouts. The winding factor of the 5-phase star

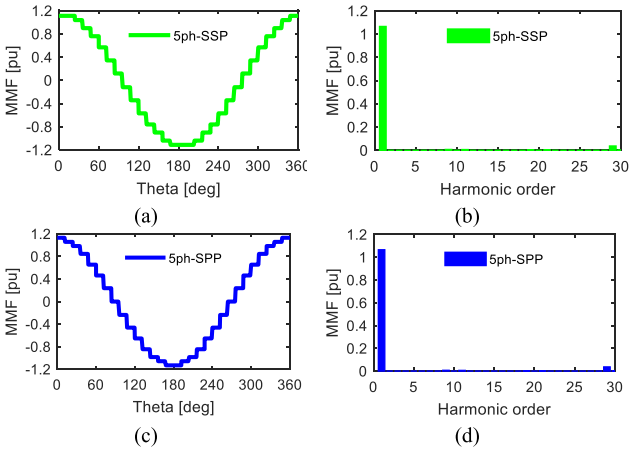

FIGURE 8. MMF magnitudes and harmonics for SSP and SPP configurations.

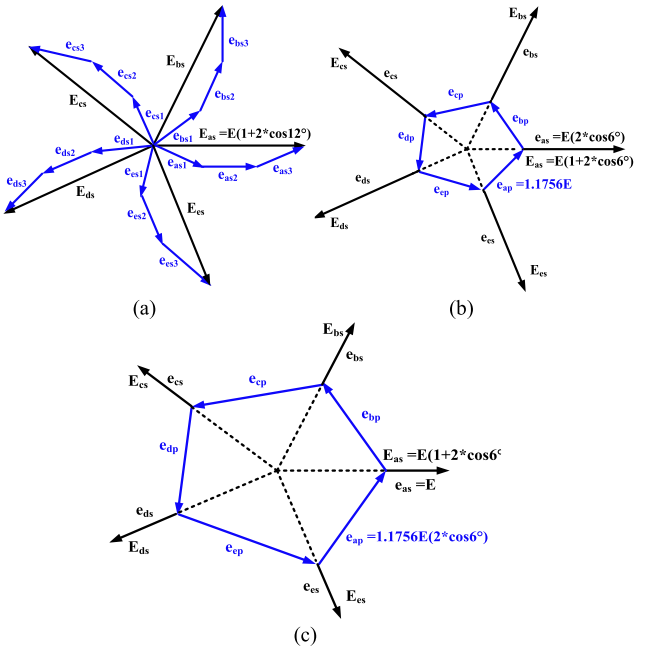

FIGURE 9. Star of slot phasor for (a) star, (b) SSP and (c) SPP configurations.

winding can be given by [23]:

$$K_w = \frac{E_{as}}{3E} \qquad (12)$$

where E_{as} and E represent the magnitude of the equivalent phase voltage of the 5-phase terminals and the magnitude of the induced EMF across each coil respectively. The winding factor of the combined star-pentagon configuration can be calculated from the same equation (12), where E_{as} can be given as described in fig.9(b and c). The winding factor for different configurations is reported in Table 4. It is noted that the winding factor of SSP and SPP layouts is increased by 3.8% compared to the 3-phase SynRM. Hence, the SynRM efficiency and torque will be improved with these configurations.

IV. MODELLING OF THE FIVE-PHASE SynRM WITH COMBINED STAR-PENTAGON WINDING

This section briefly introduces modelling of a 5-phase SynRM using the combined star-pentagon configuration. The ten components of the star and pentagon currents can be transformed to *dq*-currents as given by (13) [29]. The superscript T in (13) represents the transpose of the matrix. The value of the transformation matrix is written at the bottom of this page in (14), as shown at the bottom of the page.

$$\begin{bmatrix} i_q \\ i_d \end{bmatrix} = K_s * \begin{bmatrix} i_A & i_B & i_C & i_D & i_E & i_{EA} & i_{AB} & i_{BC} & i_{CD} & i_{DE} \end{bmatrix}^T . \tag{13}$$

The factor K_1 in (14) can be obtained when the space vector of the five components of the star and pentagon currents have the same length. To obtain the same length of the space vectors of the five components, either the pentagon currents must be multiplied by 1.1756 or the star currents must be multiplied by (1/1.1756). The second option is chosen in this paper and the value of the K_1 in (14) will be (2/10).

The dq-axis flux-linkages of the combined star-pentagon winding can be obtained using the same transformation matrix in (13) and (14). As well, K_1 will be (2/10) if the space vector of the star and pentagon flux-linkages have the same length. Hence, the flux linkages of the pentagon winding must be multiplied by (1.1756*Y). The factor Y depends on the layout of combined star-pentagon configuration: SPP or SSP. The factor Y will be 2 and 0.5 for SPP and SSP configuration respectively.

The 5-phase SynRM electromagnetic torque can be formulated by (15). The value of the factor K_2 depends on the type of winding where, it will be 1 for the conventional star connection. While, for the combined star-pentagon connection, it will be 1.5 and 3 for SPP and SSP configuration respectively.

$$T_m = \frac{5}{2} * K_2 * P * (\lambda_d i_q - \lambda_q i_d) \tag{15}$$

$$\begin{cases} \lambda_d = L_d i_d \\ \lambda_q = L_q i_q \end{cases} \tag{16}$$

The 5-phase SynRM *dq*-axis voltage equations can be described as follows [29]:

$$\begin{cases} V_d = R_s i_d - \omega_r * P * \lambda_q + \dfrac{\delta \lambda_d}{\delta t} \\ V_q = R_s i_q + \omega_r * P * \lambda_d + \dfrac{\delta \lambda_q}{\delta t} \end{cases} \tag{17}$$

The power factor (PF) of SynRM can be expressed by (18) and the torque ripple percentage ($T_r\%$) value can be computed by (18).

$$PF = \frac{V_d \cos(\alpha) + V_q \sin(\alpha)}{\sqrt{V_d^2 + V_q^2}} \tag{18}$$

$$T_r\% = \frac{max\,(T_m) - min(T_m)}{mean\,(T_m)} * 100 \tag{19}$$

The vector diagram of the 5-phase SynRM in steady state is shown in fig.10.

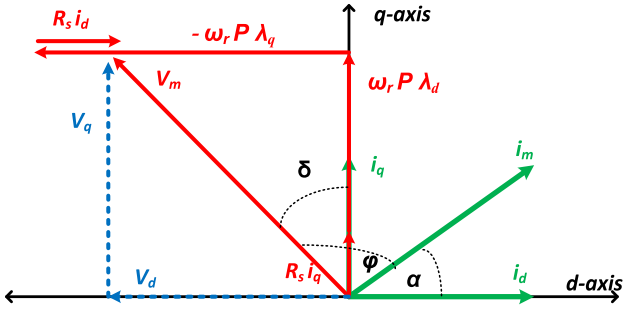

FIGURE 10. SynRM vector diagram in steady state.

V. PERFORMANCE ANALYSIS

The performance of the optimized 5-phase SynRM with different winding configurations (star and combined star-pentagon) is analyzed and compared with the existing 3-phase machine using 2D Ansys Maxwell transient simulations. This section considers three winding configurations for the 5-phase SynRM: star configuration (5ph-S) and two combined star-pentagon configurations (5ph-SSP and 5ph-SPP). Both healthy and faulty cases are considered in the following study.

A. HEALTHY CASE

The average torque of the four machines at rated speed (N = 3000 rpm), different stator currents and current angles is displayed in fig.11(a). It is noticed that the average torque increases with the increase in current angle till it reaches its maximum value at the optimal current angle. Then it decreases again. The optimal current angle is around 45° at lower currents and it increases to 55°, 58° and 56° at rated current (maximum phase current = 17.3 A) for 3ph-S, 5ph-S and the combined star pentagon configurations respectively. The increase in the current angle at higher current is due to core saturation which makes the direct axis inductance fixed

$$K_s = K_1 * \begin{bmatrix} \cos\theta_r & \cos\left(\theta_r - \frac{2\pi}{5}\right) & \cos\left(\theta_r - \frac{4\pi}{5}\right) & \cos\left(\theta_r + \frac{4\pi}{5}\right) & \cos\left(\theta_r + \frac{2\pi}{5}\right) & \cos\left(\theta_r - \frac{\pi}{10}\right) & \cos\left(\theta_r - \frac{5\pi}{10}\right) & \cos\left(\theta_r - \frac{9\pi}{10}\right) & \cos\left(\theta_r + \frac{7\pi}{10}\right) & \cos\left(\theta_r + \frac{3\pi}{10}\right) \\ \sin\theta_r & \sin\left(\theta_r - \frac{2\pi}{5}\right) & \sin\left(\theta_r - \frac{4\pi}{5}\right) & \sin\left(\theta_r + \frac{4\pi}{5}\right) & \sin\left(\theta_r + \frac{2\pi}{5}\right) & \sin\left(\theta_r - \frac{\pi}{10}\right) & \sin\left(\theta_r - \frac{5\pi}{10}\right) & \sin\left(\theta_r - \frac{9\pi}{10}\right) & \sin\left(\theta_r + \frac{7\pi}{10}\right) & \sin\left(\theta_r + \frac{3\pi}{10}\right) \end{bmatrix} \tag{14}$$

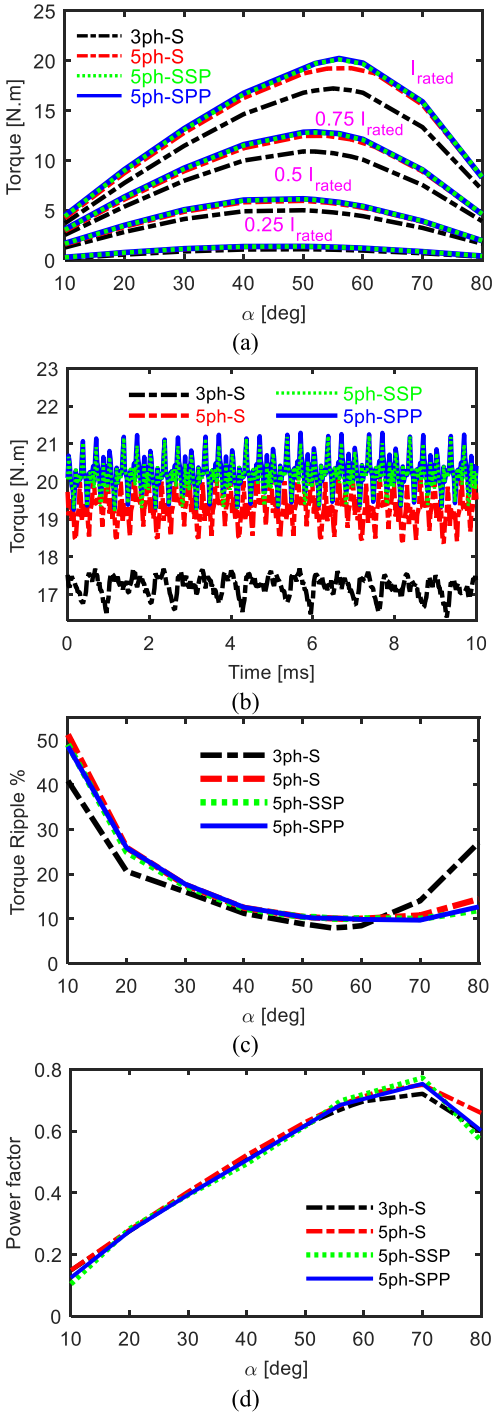

FIGURE 11. **(a) Average torque at different current angles, at different currents, and at rated speed, (b) Torque versus time at rated condition and optimal current angle, (c) Torque ripple and (d) Power factor versus current angle at rated condition.**

with further increase in current. Hence, it is better to increase the current angle to reduce direct axis current. The instantaneous torque at rated condition and optimal current angle is presented in fig.11(b). The average torque is increased from 17.23 N.m (3ph-S) to 19.26 N.m, 20.13 N.m and 20.23 N.m for 5ph-S, 5ph-SSP and 5ph-SPP respectively: an increase of 11.78%, 16.83% and 17.41% at rated conditions. The enhancement in average torque of the 5-phase SynRMs with different winding configurations is due to their high winding factor and MMF magnitude as discussed in the previous section. This is also evident when looking to the flux density distributions of the machines as shown in fig.12. Clearly, 5-phase machines show a higher flux density distribution. The torque ripple of the four studied machines at rated condition and different current angles is displayed in fig.11 (c). The torque ripple of the 3-phase SynRM is 7.94%, while it is around 10% for 5-phase SynRMs. There is a slight increase in torque ripple in the combined star-pentagon winding of the 5-phase SynRMs. This is due to the circulating currents in the pentagon winding.

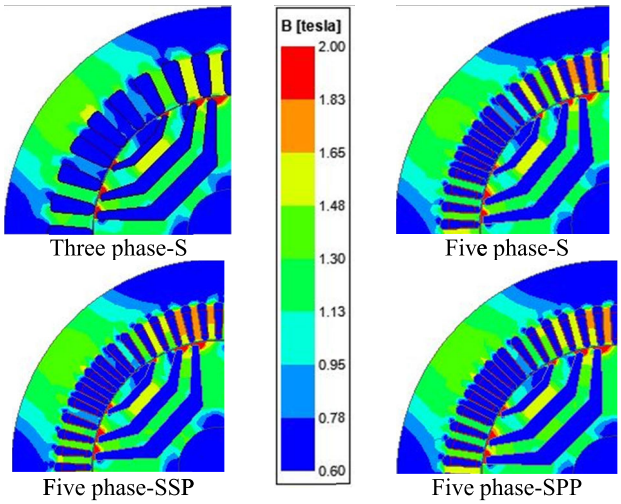

FIGURE 12. **Distribution of the flux density of the four machines at the same instant, at optimal current angle and at rated condition.**

Thanks to the enhancement in saliency difference and the higher optimal current angle, the power factor is slightly improved with the 5-phase SynRMs as reported in Table 5 and fig.11(d). Figure 11(d) shows the power factor for the four machines at different current angle and at rated condition.

TABLE 5. **Finite element simulation results.**

Parameter	3ph-S	5ph-S	5ph-SSP	5ph-SPP
T_{av} (N.m)	17.23	19.26	20.13	20.23
Torque ripple (%)	7.94	9.92	9.96	10.1
Total loss (W)	290.9	281.4	285.8	285.8
Efficiency (%)	94.88	95.56	95.68	95.70
Power Factor	0.6622	0.6989	0.6978	0.6848

Figure 13(a) shows that the 5-phase SynRMs torque gain decreases with the increase stator current. This due to the reduction of the saliency difference (Ld-Lq) with high currents. Figure 13(b) and Table 5 show that the 5-phase SynRMs have slightly lower losses compared to 3-phase SynRM. This reduction is due to their higher operating current angle compared to the 3-phase SynRM and the fact that SynRMs losses decrease with the increase in current angle as

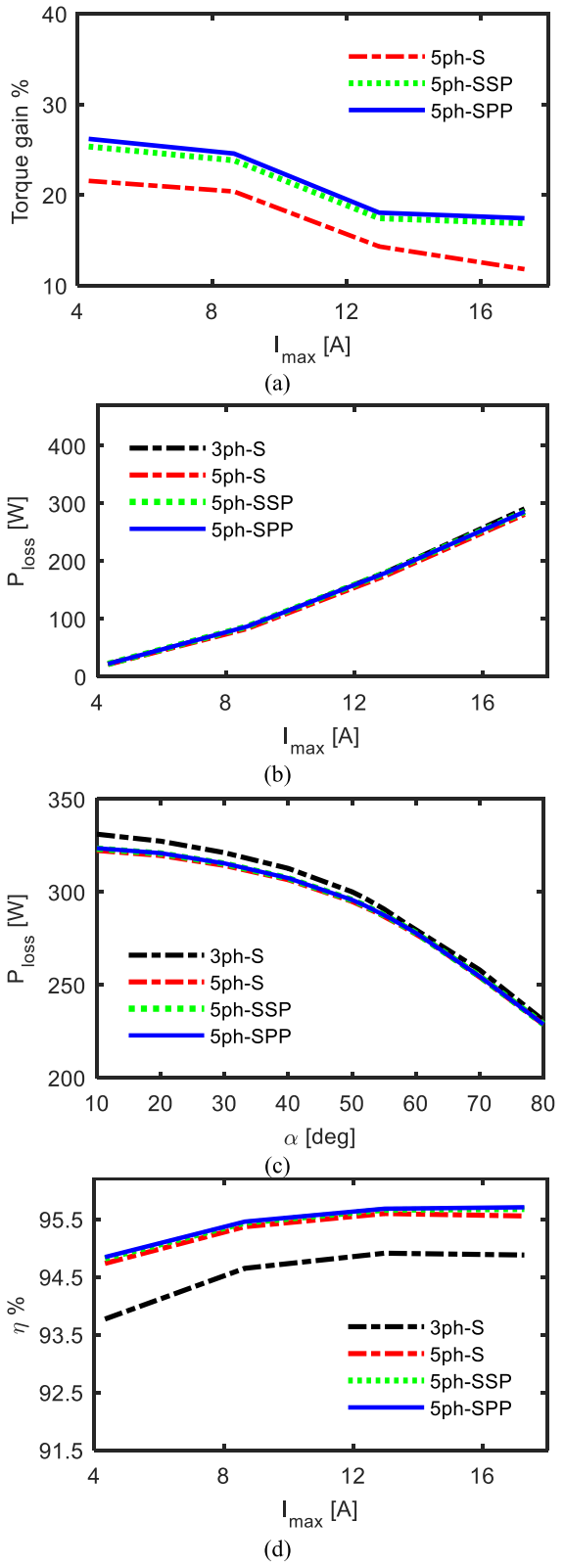

FIGURE 13. (a) Torque gain and (b) total losses versus current at optimal current angle and at rated speed (c) total losses versus current angle at rated condition (d) efficiency losses versus current at optimal current angle and at rated speed.

shown in fig.13(c). In addition, the MMF harmonic content in 5-phase SynRMs is lower compared to the harmonic content in a 3-phase SynRM as discussed in the previous section. Thanks to the slight reduction of the total losses and the significant enhancement in the average torque of the 5-phase SynRMs, the efficiency is significantly improved at rated condition from 94.88% (with 3ph-S) to 95.56%, 95.68% and 95.70% for 5ph-S, 5ph-SSP and 5ph-SPP respectively as shown in fig.13(d) and Table 5.

Figure (14) shows the line-line voltage of the four machines at optimal current angle and at rated condition. It has been found that the line voltage of the five-phase SynRMs is reduced by about 53% compared to the line voltage of the three-phase SynRM. The reduction of the line voltage in case of the five-phase SynRMs has a great advantage, where the input DC link voltage of the inverter is reduced. The DC voltage is 600 V and 300 V for the three and five-phase SynRMs respectively. This results in a lower DC link capacitor voltage, which reduces the size and the cost of the DC link capacitor and hence the drive system. This is a great advantage for specific applications like electric vehicles.

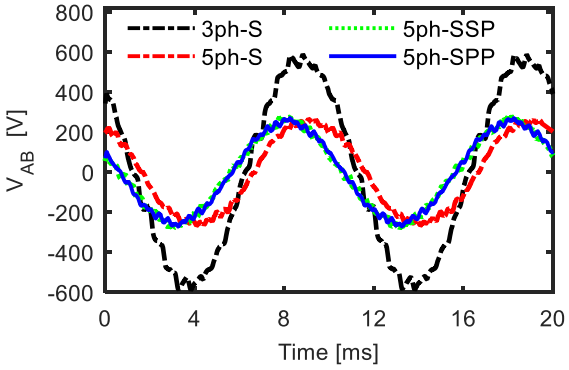

FIGURE 14. Line-line voltage at optimal current angle and at rated condition.

Figure 15 and fig.16 discuss the performance of the four machines at different speeds, optimal current angles and rated current. The optimal current angle for constant torque region ($N \leq 3000$ rpm) is the current angle that maximize the average torque. However, for over speed region ($N > 3000$ rpm), it is the angle that keeps the same rated voltage. For speed lower than rated speed, the SynRMs average torque remains fixed at different speed as shown in fig.15(a) as they operate at the same current angle and the same stator current. However, in over speed region, it decreases with the increase of the rotor speed as SynRMs operate at higher current angle to maintain fixed rated voltage. It has been found that the torque gains at 3 times the rated speed are 33.7%, 29.4% and 35.8% for 5ph-S, 5ph-SSP and 5ph-SPP respectively. A 5ph-SSP has lower torque gain compared to the other 5-phase SynRMs due to its higher current angle as shown in fig.15(b). In addition,

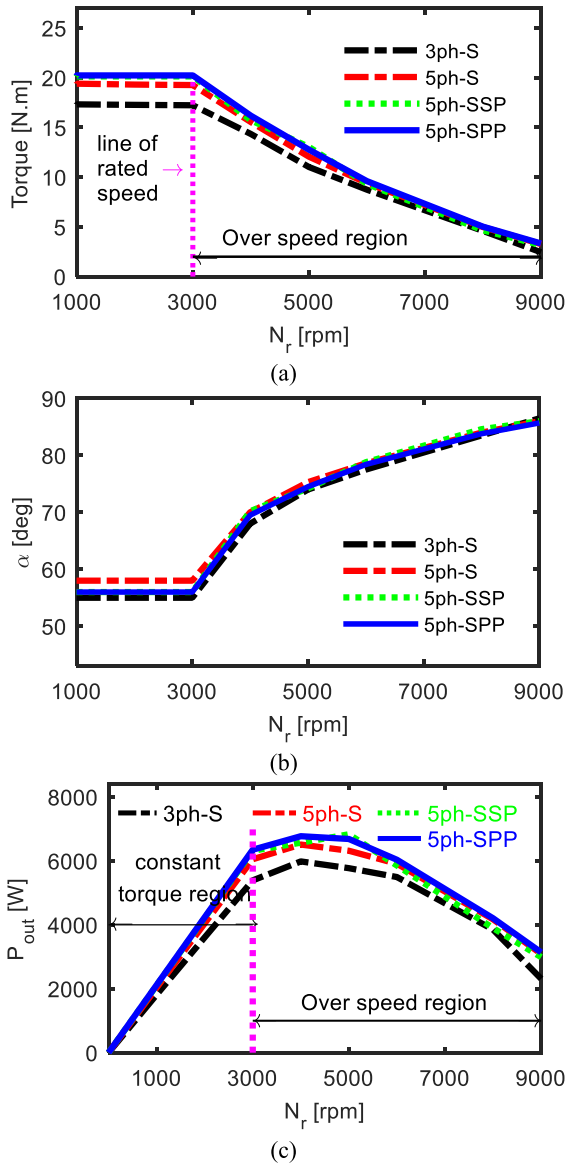

FIGURE 15. (a) Average Torque, (b) Optimal current and (c) Output power versus speed at rated current.

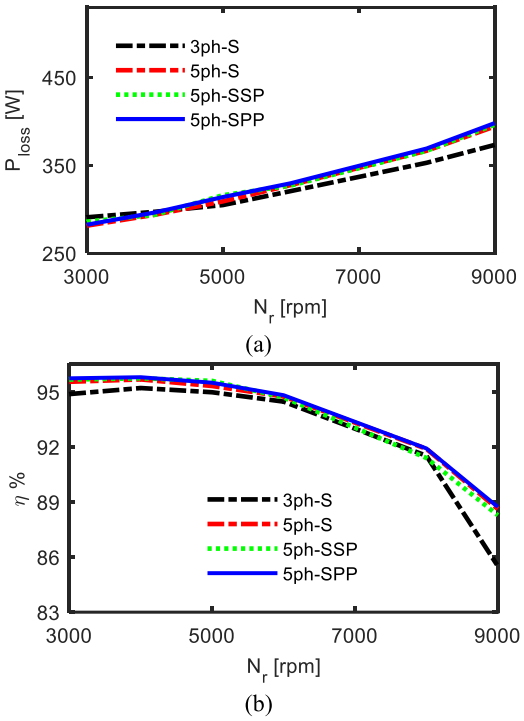

FIGURE 16. (a) Total losses and (b) Efficiency at rated current and different speeds.

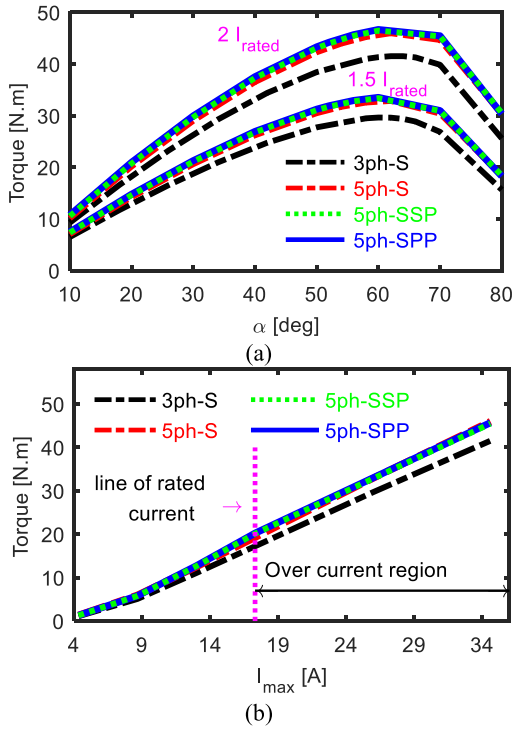

FIGURE 17. Average torque at overloading and at 1000 rpm (a) versus current angle and (b) versus line current.

these higher current angles reduce the output power in the over speed region as shown in fig.15(c). At high speeds in fig.16(a), 5-phase SynRMs have higher losses compared to 3-phase SynRM as they operate at nearly the same current angle as shown in fig.15(b), beside the small thickness of their core compared to 3-phase SynRM. fig.16(b) shows that the efficiency is greatly improved by 3.64%, 3.24% and 3.77% for 5ph-S, 5ph-SSP and 5ph-SPP respectively compared to 3ph-S.

Figure 17 studies the performance of the SynRMs at overloading for 1.5 and 2 times the rated current. It is cleared from fig.17(a) that the optimal current angle (angle gives maximum torque) is increased at overloading compared to rated condition. This is due to core saturation. Therefore, the torque gain is reduced to 10.7%, 11.9% and 12.4% for 5ph-S, 5ph-SSP and 5ph-SPP at 2 times the rated current. fig.17(b) shows that the average torque changes linearly with the stator current at optimal current angles.

TABLE 6. Simulation results for the four machines with one phase open and rated condition.

Case	Parameter	3ph-S	5ph-S	5ph-SSP	5ph-SPP
Healthy	Fund. MMF(PU)	1	1.053	1.0647	1.0647
	%THD in MMF	9.88%	3.972%	3.581%	3.581%
	T_{av} [N.m]	17.23	19.26	20.13	20.23
	T_r %	7.94%	9.92%	9.96%	10.1%
Fault	Fund. MMF(PU)	0.5774	0.9294	0.9436	0.9521
	%THD in MMF	26.13%	9.77%	7.86%	5.98%
	T_{av} [N.m]	7.47	12.62	15.06	17.03
	T_r %	228%	112%	64%	34%

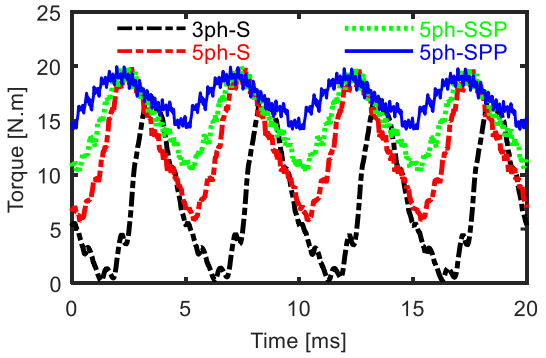

FIGURE 18. Performance at faulty case (one phase open) and rated condition.

B. FAULTY CASE

The performance of the four machines at faulty case with one phase opened is shown in fig.18. At faulty case as described in Table 6, it is seen that the MMF magnitude is reduced by 42.26%, 7.06%, 5.64% and 4.79% for 3ph-S, 5ph-S, 5ph-SSP and 5ph-SPP respectively compared to the healthy case of 3ph-S. In addition, the MMF harmonics (THD) are increased to 26.13%, 9.77%, 7.86% and 5.89% for 3ph-S, 5ph-S, 5ph-SSP and 5ph-SPP respectively. Consequently, the SynRM's average torque at faulty case (with one phase opened) for 3ph-S, 5ph-S, 5ph-SSP and 5ph-SPP is 43.35%, 73.24%, 87.41% and 98.84% of the healthy rated value of 3ph-S. In addition, the torque ripple of the 5-phase SynRMs at faulty case is lower compared to 3-phase SynRM and 5ph-SSP has the lowest torque ripple of 34%. The torque ripple of 3ph-S, 5ph-S and 5ph-SSP at faulty case is 228%, 112% and 64% respectively. The high torque ripple at faulty case of the 3-phase SynRM produces higher vibrations and noise with mechanical problems. Finally, the reduction in average torque and the increase in torque ripple agree with MMF analyses in Table 6. However, the proposed 5-phase SynRMs in this paper offers an acceptable torque ripple at faulty case compared to the 3-phase SynRM. The torque ripple of the proposed SynRMs could be further improved by applying the control strategy introduced in [30].

C. COMPARATIVE ANALYSIS

Table 7 shows the comparison of the proposed 5-phase SynRMs with the proposed SynRM in a previous study [31]. However, the proposed SynRM in [31] offers a smooth torque ripple as it provides an improved quality MMF. The proposed 5-phase SynRM with the new winding in this paper offers a high MMF magnitude with lower harmonics as shown in fig (8). The proposed SynRM in [31] requires a special type of power electronic converter with higher number of semiconductors switches compared to the proposed 5-phase SynRMs in this paper [32], [33]. The proposed multiphase SynRM in [31] has a higher fault tolerance because of non-overlap winding and the higher number of phase (42-phase). Nevertheless, this complicates the drive system. However, the proposed 5-phase SynRM in this paper offers an improved performance at faulty case as introduced in the previous section without complicating the drive system. In addition, the maximum possible value of the efficiency in [31] is 94.1% compared to 95.7% of the 5ph-SPP. This is due to the different types of losses as reported in [31]. However, the power factor of the machine in [31] has slightly high values and can be improved with the modification of the control strategy.

TABLE 7. Comparison with another topology.

	5ph-SSP	5ph-SPP	SynRM in [31]
Stator winding	coils and stranded conductors.		stator cage and solid conductors
Conductor material	copper		aluminium
Applications	electric vehicles and hospital pumping		low voltage high power electric vehicles
Number of slots	60		42
Number of rotor poles	4		6
Number of phases	5		42
Number of turns per phase	48		0.5
DC-link voltage	300V		60V
Power electronic converter	Conventional inverter is used		Special type of inverter with high number of semiconductors
Efficiency	95.68%	95.70%	94.10%
Power factor	0.6978	0.6848	0.76

VI. EXPERIMENTAL RESULTS

In order to validate the analytical and finite element models that are employed before, the experimental set up shown in Fig. 19 is used. The reference 3-phase SynRM of 36 slots, 4 poles and 5.5 kW is tested. The 3-phase SynRM is coupled with 3-phase 10 kW induction motor. A Lorenz torque sensor is inserted in the coupling system between the two machines to measure the SynRM torque. The speed is measured using an incremental encoder fixed in the rotor of the induction motor. The 3-phase SynRM operates in torque control mode and its speed is controlled using the induction motor. A 3-phase inverter is used to control the 3-phase SynRM with

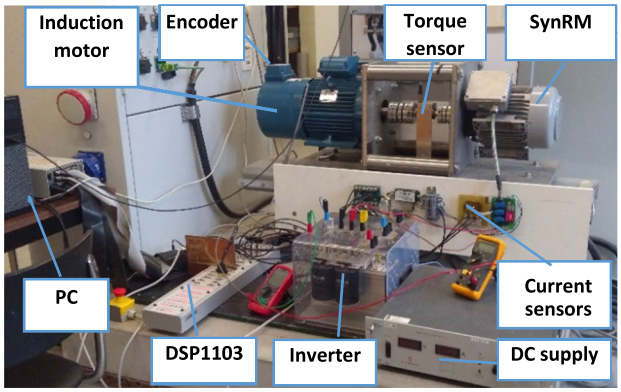

FIGURE 19. The complete experimental test bench.

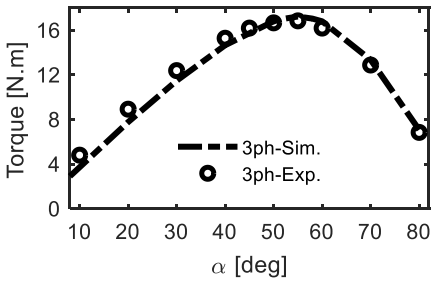

FIGURE 20. Measured and simulated average torque versus current angle at rated condition.

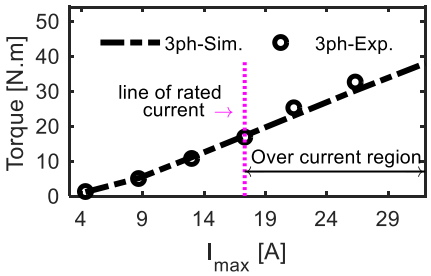

FIGURE 21. Measured and simulated average torque versus line current at optimal current angles and $N_r = 1000rpm$.

switching frequency of 6.6 kHz. The DC bus voltage is 600 V. By means of digital signal processing (DSP1103), a space vector pulse width modulation with field-oriented control is applied to obtain the inverter controlling pulses.

Figure 20 shows the measured and simulated average torque of the 3-phase SynRM at rated condition and different current angle. There is an acceptable agreement between the measured and simulated results in fig.20. The simulated and measured average torque of the 3-phase SynRM at different line current including overloading condition and 1000 rpm is shown in fig.21. It has been found from fig.21 that the average torque varies linearly with the line current. Figure 22 shows the measured and simulated losses, efficiency and power factor of the 3-phase SynRM at rated different line current, at optimal current angle and at rated speed. The slight difference between the simulated and measured losses and efficiency is due to neglecting the mechanical and

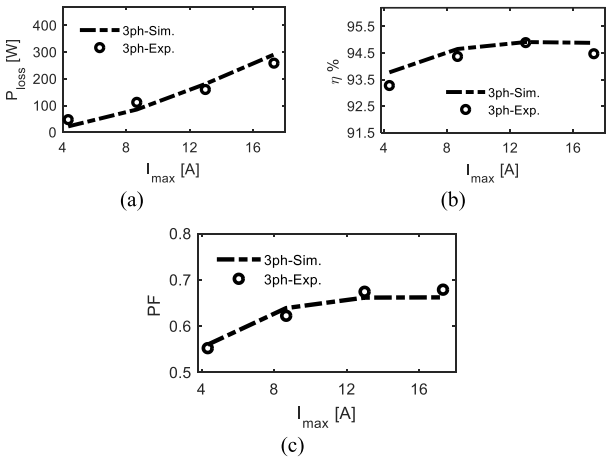

FIGURE 22. (a) Total losses, (b) Efficiency and (c) Power factor versus stator current at rated speed and optimal current angle.

switching losses in simulation results and the accuracy of both torque sensor and the incremental encoder. The change in the power factor between low and high currents in fig.22(c) is due to the change of the optimal current angle with the variation of line current.

Figures 20-22 prove that the implemented models are experimentally valid.

VII. CONCLUSION

The performance of the 3-phase SynRM has been improved by upgrading its stator to 5-phase keeping the same rotor. The upgraded 5-phase stator has been optimized with the existing rotor to select the optimal dimensions of the slot and teeth. Moreover, the optimized 5-phase SynRM has been extra improved using a combined star pentagon winding. Different winding configurations have been studied and compared using 2D Ansys Maxwell transient simulations. It has been found that the average torque and efficiency are increased by 17.41% and 0.86% respectively for 5ph-SPP compared to the 3ph-S at optimal current angle and at rated condition. At 3 times the rated speed, the torque and efficiency are significantly increased by 35.8% and 3.77% respectively for 5ph-SPP compared to the 3ph-S. The torque gain at overloading with double the rated current is 12.4% for 5ph-SPP compared to 3ph-S. Moreover, 5-phase SynRMs proved better performance at faulty case with one phase opened. It works at 98.84% of the healthy rated value of 3ph-S, whereas the 3ph-S works at only 43.35% with huge torque ripple (228%). Finally, an experimental validation for the reference machine has been done and compared with the simulated results.

REFERENCES

[1] W. Zhao, D. Chen, T. A. Lipo, and B.-I. Kwon, "Performance improvement of ferrite-assisted synchronous reluctance machines using asymmetrical rotor configurations," *IEEE Trans. Magn.*, vol. 51, no. 11, pp. 1–4, Nov. 2015.

[2] E. Howard, M. J. Kamper, and S. Gerber, "Asymmetric flux barrier and skew design optimization of reluctance synchronous machines," *IEEE Trans. Ind. Appl.*, vol. 51, no. 5, pp. 3751–3760, Sep. 2015.

[3] M. N. Ibrahim, P. Sergeant, and E. E. M. Rashad, "Combined star-delta windings to improve synchronous reluctance motor performance," *IEEE Trans. Energy Convers.*, vol. 31, no. 4, pp. 1479–1487, Dec. 2016.
[4] J. Baek, S. S. R. Bonthu, and S. Choi, "Design of five-phase permanent magnet assisted synchronous reluctance motor for low output torque ripple applications," *IET Electr. Power Appl.*, vol. 10, no. 5, pp. 339–346, May 2016.
[5] M. N. Ibrahim, P. Sergeant, and E. M. Rashad, "Synchronous reluctance motor performance based on different electrical steel grades," *IEEE Trans. Magn.*, vol. 51, no. 11, Nov. 2015, Art. no. 7403304.
[6] N. Bianchi, S. Bolognani, D. Bon, and M. Dai Pre, "Torque harmonic compensation in a synchronous reluctance motor," *IEEE Trans. Energy Convers.*, vol. 23, no. 2, pp. 466–473, Jun. 2008.
[7] E. Castagnaro, G. Bacco, and N. Bianchi, "Impact of geometry on the rotor iron losses in synchronous reluctance motors," *IEEE Trans. Ind. Appl.*, vol. 55, no. 6, pp. 5865–5872, Nov. 2019.
[8] R.-R. Moghaddam and F. Gyllensten, "Novel high-performance SynRM design method: An easy approach for a complicated rotor topology," *IEEE Trans. Ind. Electron.*, vol. 61, no. 9, pp. 5058–5065, Sep. 2014.
[9] S. Taghavi and P. Pillay, "A novel grain-oriented lamination rotor core assembly for a synchronous reluctance traction motor with a reduced torque ripple algorithm," *IEEE Trans. Ind. Appl.*, vol. 52, no. 5, pp. 3729–3738, Sep. 2016.
[10] C. Babetto, G. Bacco, and N. Bianchi, "Synchronous reluctance machine optimization for high-speed applications," *IEEE Trans. Energy Convers.*, vol. 33, no. 3, pp. 1266–1273, Sep. 2018.
[11] K. Wang, Z. Y. Gu, C. Liu, and Z. Q. Zhu, "Design and analysis of a five-phase SPM machine considering third harmonic current injection," *IEEE Trans. Energy Convers.*, vol. 33, no. 3, pp. 1108–1117, Sep. 2018.
[12] Y. Hu, Z. Q. Zhu, and M. Odavic, "Comparison of two-individual current control and vector space decomposition control for dual three-phase PMSM," *IEEE Trans. Ind. Appl.*, vol. 53, no. 5, pp. 4483–4492, Sep. 2017.
[13] M. J. Duran, E. Levi, and F. Barrero, "Multiphase electric drives: Introduction," in *Wiley Encyclopedia of Electrical and Electronics Engineering*. Hoboken, NJ, USA: Wiley, 2017. [Online]. Available: https://doi.org/10.1002/047134608X.W8364
[14] M. Muteba, "Influence of mixed stator winding configurations and number of rotor flux-barriers on torque and torque ripple of five-phase synchronous reluctance motors," *IEEE Transp. Electrific. Conf. Expo (ITEC)*, Detroit, MI, USA, Jun. 2019, pp. 1–6.
[15] K. B. Tawfiq, M. N. Ibrahim, E. E. EL-Kholy, and P. Sergeant, "Refurbishing three-phase synchronous reluctance machines to multi-phase machines," *Electr. Eng.*, to be published, doi: 10.1007/s00202-020-01064-w.
[16] S. Sadeghi, L. Guo, H. A. Toliyat, and L. Parsa, "Wide operational speed range of five-phase permanent magnet machines by using different stator winding configurations," *IEEE Trans. Ind. Electron.*, vol. 59, no. 6, pp. 2621–2631, Jun. 2012.
[17] A. S. Abdel-Khalik, M. A. Elgenedy, S. Ahmed, and A. M. Massoud, "An improved fault-tolerant five-phase induction machine using a combined Star/Pentagon single layer stator winding connection," *IEEE Trans. Ind. Electron.*, vol. 63, no. 1, pp. 618–628, Jan. 2016.
[18] A. S. Abdel-Khalik, S. Ahmed, and A. M. Massoud, "Dynamic modeling of a five-phase induction machine with a combined Star/Pentagon stator winding connection," *IEEE Trans. Energy Convers.*, vol. 31, no. 4, pp. 1645–1656, Dec. 2016.
[19] A. S. Abdel-Khalik, S. Ahmed, and A. M. Massoud, "Steady-state mathematical modeling of a five-phase induction machine with a combined star/pentagon stator winding connection," *IEEE Trans. Ind. Electron.*, vol. 63, no. 3, pp. 1331–1343, Mar. 2016.
[20] A. Chen, R. Nilssen, and A. Nysveen, "Harmonic analysis and comparison of the back EMFs of four permanent magnet machines with different winding arrangements," in *Proc. Int. Conf. Electr. Mach. Syst., Wuhan*, Oct. 2008, pp. 3043–3048.
[21] A. Alaeddini and H. Tahanian, "Effect of number of phases on electromagnetic torque of synchronous machines," *Int. J. Electr. Energy*, vol. 2, no. 3, pp. 194–199, Sep. 2014.
[22] M. Ibrahim, P. Sergeant, and E. Rashad, "Simple design approach for low torque ripple and high output torque synchronous reluctance motors," *Energies*, vol. 9, no. 11, p. 942, Nov. 2016.
[23] M. N. F. Ibrahim, A. S. Abdel-Khalik, E. M. Rashad, and P. Sergeant, "An improved torque density synchronous reluctance machine with a combined star–delta winding layout," *IEEE Trans. Energy Convers.*, vol. 33, no. 3, pp. 1015–1024, Sep. 2018.
[24] P. G. Artetxe, J. Paredes, B. Prieto, M. Martinez-Iturralde, and I. Elosegui, "Optimal pole number and winding designs for low speed-high torque synchronous reluctance machines," *Energies*, vol. 11, no. 128, pp. 1–21, 2018.
[25] W. Han, C. Van Dang, J.-W. Kim, Y.-J. Kim, and S.-Y. Jung, "Global-simplex optimization algorithm applied to FEM-based optimal design of electric machine," *IEEE Trans. Magn.*, vol. 53, no. 6, pp. 1–4, Jun. 2017.
[26] F. Cupertino, G. Pellegrino, and C. Gerada, "Design of synchronous reluctance motors with multiobjective optimization algorithms," *IEEE Trans. Ind. Appl.*, vol. 50, no. 6, pp. 3617–3627, Nov. 2014.
[27] V. Prakht, V. Dmitrievskii, V. Kazakbaev, S. Oshurbekov, and M. N. Ibrahim, "Optimal design of a novel three-phase high-speed flux reversal machine," *Appl. Sci.*, vol. 9, no. 3822, pp. 1–14, 2019.
[28] M. J. Kamper, F. S. Van der Merwe, and S. Williamson, "Direct finite element design optimisation of the cageless reluctance synchronous machine," *IEEE Trans. Energy Convers.*, vol. 11, no. 3, pp. 547–555, Sep. 1996.
[29] A. Vagati, "The synchronous reluctance solution: A new alternative in AC drives," in *Proc. 20th Annu. Conf. IEEE Ind. Electron. IECON*, Sep. 1994, pp. 1–13.
[30] G. Liu, J. Ni, and Q. Chen, "Fault tolerant control for five-phase synchronous reluctance motor by third harmonic current injection," in *Proc. Chin. Intell. Automat. Conf. CIAC* in Lecture Notes in Electrical Engineering, vol. 586, Z. Deng, Ed. Singapore: Springer, 2020, pp. 529–536.
[31] V. Bilyi, D. Bilyi, O. Moros, G. Dajaku, and D. Gerling, "Synchronous reluctance machine with multiphase stator cage winding," in *Proc. 20th Int. Conf. Electr. Mach. Syst. (ICEMS)*, Aug. 2017, pp. 1–6, doi: 10.1109/ICEMS.2017.8056518.
[32] A. Patzak and D. Gerling, "Design of a multi-phase inverter for low voltage high power electric vehicles," in *Proc. IEEE Int. Electr. Vehicle Conf. (IEVC)*, Dec. 2014, pp. 1–7, doi: 10.1109/IEVC.2014.7056143.
[33] B. Rubey and D. Gerling, "Design of high current low voltage half-bridges for multi-phase inverter application in the ISCAD drive," in *Proc. 19th Int. Conf. Electr. Mach. Syst. (ICEMS), Chiba*, Nov. 2016, pp. 1–6.

KOTB B. TAWFIQ received the B.Sc. and M.Sc. degrees in electrical engineering from the Faculty of Engineering, Menoufia University, Egypt, in 2013 and 2016, respectively. He is currently pursuing the Ph.D. degree with Ghent University, Belgium. He is an Assistant Lecturer with the Department of Electrical Engineering, Faculty of Engineering, Menoufia University. His main fields of interest include power electronics, matrix converters, renewable energy, electrical machines drives, and design and control of electrical machines. He serves as a Reviewer of several journals and conferences.

MOHAMED N. IBRAHIM (Member, IEEE) received the B.Sc. degree in electrical power and machines engineering from Kafrelshiekh University, Egypt, in 2008, the M.Sc. degree in electrical power and machines engineering from Tanta University, Egypt, in 2012, and the Ph.D. degree in electromechanical engineering from Ghent University, Belgium, in 2017. In 2008, he became a Teaching Assistant with the Department of Electrical Engineering, Kafrelshiekh University. He is currently working as a Postdoctoral Researcher with the Department of Electromechanical, Systems, and Metal Engineering, Ghent University. He is also an Assistant Professor (on leave) with the Department of Electrical Engineering, Kafrelshiekh University. His major research interests include design and control of electrical machines and drives for industrial and sustainable energy applications. He received the Kafrelshiekh University Award several times, for his international scientific publications. He serves as a Reviewer of several journals and conferences, including the IEEE TRANSACTIONS ON INDUSTRIAL ELECTRONICS, the IEEE TRANSACTIONS ON INDUSTRY APPLICATIONS, and the IEEE TRANSACTIONS ON MAGNETICS. He also serves as a Guest Editor for the special issue of *Energies* journal.

E. E. EL-KHOLY (Member, IEEE) received the B.Sc., M.Sc., and Ph.D. degrees in electrical engineering from the Faculty of Engineering, Menoufia University, in 1986, 1992, and 1996, respectively. He is the Dean of the Faculty of Engineering, Menoufia University, and the President of Delta University. His main fields of interests include power electronics, ac/dc drives control techniques, active rectifiers, active filters, microgrids, renewable energy, real-time control using DSP, and fuzzy applications in power electronics.

PETER SERGEANT (Senior Member, IEEE) received the M.Sc. degree in electromechanical engineering and the Ph.D. degree in engineering sciences from Ghent University, Ghent, Belgium, in 2001 and 2006, respectively. He is a Professor of electrical drives with Ghent University and the Manager of cluster motion products with the Core Lab EEDT-MP, FlandersMake@UGent. He became a Postdoctoral Researcher with Ghent University, in 2006 (Postdoctoral Fellow of the Research Foundation of FlandersMake@UGent). Since 2012, he has been an Associate Professor with Ghent University. His current research domains are electrical machines and drives for industrial and sustainable energy applications.